International Journal of Nanomedicine

Dovepress
open access to scientific and medical research

Open Access Full Text Article

ORIGINAL RESEARCH

US/MR Bimodal Imaging-Guided Bio-Targeting Synergistic Agent for Tumor Therapy

Fujie Jiang[1,2,*], Lu Wang[1,*], Yu Tang[1], Yaotai Wang[1], Ningshan Li[1,3], Disen Wang[1], Zhong Zhang[1], Li Lin[1], Yan Du[1], Xia Ou[1], Jianzhong Zou[1]

[1]State Key Laboratory of Ultrasound in Medicine and Engineering, Chongqing Key Laboratory of Biomedical Engineering, College of Biomedical Engineering, Chongqing Medical University, Chongqing, People's Republic of China; [2]Department of Radiology, Chongqing University Cancer Hospital, School of Medicine, Chongqing University, Chongqing, People's Republic of China; [3]Department of Ultrasound, Xinqiao Hospital of Army Medical University, Chongqing, People's Republic of China

*These authors contributed equally to this work

Correspondence: Jianzhong Zou, State Key Laboratory of Ultrasound in Medicine and Engineering, Chongqing Key Laboratory of Biomedical Engineering, College of Biomedical Engineering, Chongqing Medical University, Chongqing, People's Republic of China, Tel +86-13708302390, Email zoujzh@cqmu.edu.cn

Purpose: Breast cancer is detrimental to the health of women due to the difficulty of early diagnosis and unsatisfactory therapeutic efficacy of available breast cancer therapies. High intensity focused ultrasound (HIFU) ablation is a new method for the treatment of breast tumors, but there is a problem of low ablation efficiency. Therefore, the improvement of HIFU efficiency to combat breast cancer is immediately needed. This study aimed to describe a novel anaerobic bacteria-mediated nanoplatform, comprising synergistic HIFU therapy for breast cancer under guidance of ultrasound (US) and magnetic resonance (MR) bimodal imaging.

Methods: The PFH@CL/Fe_3O_4 nanoparticles (NPs) (Perfluorohexane (PFH) and superparamagnetic iron oxides (SPIO, Fe_3O_4) with cationic lipid (CL) NPs) were synthesized using the thin membrane hydration method. The novel nanoplatform *Bifidobacterium bifidum*-mediated PFH@CL/Fe_3O_4 NPs were constructed by electrostatic adsorption. Thereafter, US and MR bimodal imaging ability of *B. bifidum*-mediated PFH@CL/Fe_3O_4 NPs was evaluated in vitro and in vivo. Finally, the efficacy of HIFU ablation based on *B. bifidum*-PFH@CL/Fe_3O_4 NPs was studied.

Results: *B. bifidum* combined with PFH@CL/Fe_3O_4 NPs by electrostatic adsorption and enhanced the tumor targeting ability of PFH@CL/Fe_3O_4 NPs. US and MR bimodal imaging clearly displayed the distribution of the bio-targeting nanoplatform in vivo. It was conducive for accurate and effective guidance of HIFU synergistic treatment of tumors. Furthermore, PFH@CL/Fe_3O_4 NPs could form microbubbles by acoustic droplet evaporation and promote efficiency of HIFU ablation under guidance of bimodal imaging.

Conclusion: A bio-targeting nanoplatform with high stability and good physicochemical properties was constructed. The HIFU synergistic agent achieved early precision imaging of tumors and promoted therapeutic effect, monitored by US and MR bimodal imaging during the treatment process.

Keywords: high-intensity focused ultrasound, nanoparticles, *Bifidobacterium bifidum*, imaging guidance, cancer therapy

Introduction

The treatment of breast cancer is facing the big challenge of insufficient treatment. High intensity focused ultrasound (HIFU) has shown unprecedented potential for cancer treatment and widely used in treating primary and metastatic solid tumors.[1,2] Theoretically, HIFU increases the temperature of target tissues by focusing ultrasonic energy.[3–5] However, because ultrasound energy attenuates with increasing treatment depth, ultrasound energy deposition is usually insufficient in deep and large tumor tissues.[6] Therefore, improving the efficiency of treatment while reducing damage to normal tissues is challenging. The introduction of gaseous HIFU synergistic agents enhances the ultrasonic cavitation effect and improves the effect of HIFU ablation.[7] The most widely used substances are perfluorocarbons (PFH) with low boiling point (56°C) liquid–gas phase transition properties, which are used for synthesizing nanoscale HIFU synergistic agents.[8–14] Nano drug delivery system has been widely used in the treatment of tumors,[15–18] but the HIFU synergist developed based on nanomaterials still has some

Received: 15 March 2022
Accepted: 26 June 2022
Published: 4 July 2022

problems of poor targeting and loss to normal tissues. Moreover, HIFU treatment is inseparable from image monitoring, but single ultrasound imaging makes it hard to meet the growing demand for HIFU treatment. Therefore, we need to find a more optimal method to actively target delivery of synergists and increase the accumulation of synergists in tumors. At the same time, it is necessary to introduce a non-invasive multimodal monitoring method to monitor the treatment process in real time.

The accumulation of synergistic agents in targeted tissues is the key for improving therapeutic efficiency of HIFU ablation. Therefore, tumor targeting properties of HIFU synergistic agents should be improved. The use of live tumor-targeting bacterial vectors as natural "microrobots" is a potential strategy for cancer therapy. *Bifidobacterium bifidum*,[19,20] *Salmonella typhimurium*,[21] *Escherichia coli*,[22,23] and other anaerobic bacteria have been widely used in cancer treatment due to their good biosafety and biocompatibility properties. Theoretically, the unique structure of a tumor site determines the hypoxic characteristics of the tumor microenvironment, and anaerobic *B. bifidum* is highly selective and can deeply colonize hypoxic tumor sites.[24,25] Bacterial colonization in tumors can improve retention efficiency and prolong retention time of lipid nanoparticles.[26,27] In addition, functional nanomaterial-modified anaerobic *B. bifidum* can enhance the effect of precise tumor targeting therapy and early imaging.[28]

Multimodal imaging probes or contrast agents need to be introduced into the nanoplatform to ensure accurate HIFU therapy.[29] Each imaging technique has its inherent limitations, however, such as the relatively low sensitivity of magnetic resonance (MR) imaging and the low resolution of ultrasound (US) imaging. Therefore, developing novel imaging contrast agents that integrate the distinct strengths of different imaging techniques would be valuable for biomedical diagnosis.[30] Bimodal imaging provides more detailed diagnostic information than unimodal imaging. US and MR imaging can accurately assess the therapeutic effect of HIFU ablation. Accurate tumor diagnosis can improve prognosis and survival rate. Therefore, combining US and MR imaging is extremely important in cancer diagnosis.

In this study, a *B. bifidum*-mediated nanoplatform was constructed for HIFU ablation of tumors under the guidance of multimodal imaging. First, cationic liposomes have the advantages of good biodegradability, easy surface modification, and prolonged circulation time. They are widely used as imaging agents and nanodelivery carriers for anti-tumor drugs. Second, liquid PFH was vaporized into microbubbles by acoustic drop vaporization (ADV) to enhance ultrasonic cavitation and achieve synergistic HIFU treatment. Additionally, superparamagnetic iron oxides (SPIO, Fe_3O_4) were integrated into the shell of liposomal nanoparticles (NPs) to enhance T_2-weighted MRI capability of NPs. Finally, *B. bifidum* was connected with PFH@CL-Fe_3O_4 NPs by electrostatic adsorption to construct the bio-targeting nanoplatform.

Materials and Methods

Materials

Lipids, including 1,2-dipalmitoyl-sn-glycero-3-phosphocho-line (DPPC), 1,2-distearoyl-sn-glycero-3-phosphoethanola-mine -N-[amino(polyethyleneglycol)-2000] (DSPE-PEG2000-Amine), and DC-cholesterol hydrochloride (DC-CHOL) were purchased from Avanti Polar Lipids (Alabaster, AL, USA). Chloroform ($CHCl_3$) was purchased from Chongqing East Chemical Industry Ltd, Co. (Chongqing, China). Superparamagnetic iron oxide nanoparticles (Fe_3O_4, 10 nm, 25 mg/mL) were purchased from Ocean Nanotech Co. Ltd. (San Diego, USA). Perfluorohexanes (PFH, a PFC compound with a boiling point of 56°C) were purchased from Biofroxx Ltd, Co. (Shanghai, China). 1,1′-dioctadecyl-3,3,3′,3′-tetramethylindotricarbocyanine iodide (DiR) was purchased from AAT Bioquest Inc. (USA). 2-(4-Amidinophenyl)- 6-indolecarbamidinedihyrochloride(DAPI), 1,1-dioctadecyl-3,3,3′,3′-tetramethylindocarbocyanine perchlorate (DiI) and fluorescein isothiocyanate (FITC) were purchased from Beyotime Biotechnology Co., Ltd (Shanghai, China).

Methods

Preparation and Synthesis of PFH@CL/Fe_3O_4 NPs

The cationic liposomal (CL) nanoparticles encapsulating Fe_3O_4 and PFH were prepared by thin film hydration methods.[31] First, 6 mg DPPC, 2 mg DSPE-PEG (2000)-amine, and 2 mg DC-cholesterol were dissolved in 10 mL $CHCl_3$. Thereafter, 200 μL Fe_3O_4 NPs were added sequentially. In an ice bath, the mixture was emulsified using a rotary evaporator (Yarong Inc., Shanghai, China) to remove the organic solvent and form the lipid films at a temperature of 52°C for 1 h. Subsequently, 200 μL PFH was added into lipid films and sonicated using an ultrasonic probe (Sonics and Materials, Inc., USA) at 100 W for 5 min.

After the prepared emulsion was centrifuged at 8000 rpm for 5 min, the supernatant was discarded. The precipitate of Fe_3O_4 and PFH was washed using deionized water. The process was repeated thrice. Finally, the precipitate was dissolved in 2 mL deionized water and lyophilized for 48 h. The dried samples were stored at 4°C for further use. PFH/CL NPs, Fe_3O_4/CL NPs, and CL NPs were prepared using a similar procedure without adding PFH or Fe_3O_4 NPs. To prepare fluorescent NPs, the fluorescent dye, DiI or DiR was added to the organic phase in the dark.

B. bifidum Culture

B. bifidum strain, ATCC 29521 (*B. bifidum*, American Type Culture Collection), was cultured in Man–Rogosa–Sharpe (MRS) broth in a hypoxic environment created using an anaerobic airbag-anoxic closed system for 18 h at 37°C. Colony forming units (CFUs) were counted. *B. bifidum* was collected by centrifugation at 4°C (1000 rpm, 5 min) and washed thrice. *B. bifidum* was resuspended in PBS until the concentration was adjusted to 1×10^6 CFU/mL.

Characterization of PFH@CL/Fe_3O_4 NPs and *B. bifidum*

The structure and morphologic characterization of PFH@CL/Fe_3O_4 NPs were observed under the transmission electron microscope (TEM, Hitachi H-7600, Japan) and optical microscope (Olympus BX51, Japan). The average particle size distribution, zeta potential of the PFH@CL/Fe_3O_4 NPs, and zeta potential of *B. bifidum* were determined by a dynamic laser light scattering system (DLS, Malvern Instruments, UK). The stability of mean particle size and zeta potential of the NPs dissolved in PBS were measured within 9 days. The PFH@CL/Fe_3O_4 NPs were dissolved in dimethysulfoxide; thereafter, 36% HCl was added to the solution to decompose Fe_3O_4. The solution containing Fe was diluted with 1% HCl. The concentration of Fe_3O_4 in PFH@CL/Fe_3O_4 NPs was measured using the atomic absorption spectrometer (Hitachi model Z-5000, Hitachi Ltd, Japan). The encapsulation efficiency of Fe_3O_4 was calculated with the following equation: Encapsulation efficiency (%) = (the mass of Fe_3O_4 in sample)/(the total mass of Fe_3O_4) × 100%

Construction of the Biological Target Magnetic NPs

The biological target magnetic NPs were constructed by the ligation of PFH@CL/Fe_3O_4 nanoparticles and *B. bifidum* by electrostatic adsorption. The PFH@CL/Fe_3O_4 NPs (1 mg/mL) and *B. bifidum* (1×10^6 CFU/mL) were mixed at the ratio of 10:1. Afterwards, the mixture is incubated at room temperature for 5 min. The resulting *B. bifidum*-NP bioconjugates were centrifuged and washed with PBS for three times to remove unreacted NPs. The experimental details of TEM and DLS of *B. bifidum*-NP bioconjugates can be found in the Supporting Information 1.1.

To observe the connection between PFH@CL/Fe_3O_4 NPs and *B. bifidum*, the samples were divided into the targeted group (PFH@CL/Fe_3O_4 NPs + *B. bifidum*) and non-targeted group (PFH/Lip/Fe_3O_4 NPs + *B. bifidum*). The targeted group was treated with 1×10^6 CFU/mL FITC-labeled *B. bifidum* and 1 mg/mL DiI-labeled PFH@CL/Fe_3O_4 NPs, whereas the non-targeted group was treated with 1×10^6 CFU/mL FITC-labeled *B. bifidum* and 1 mg/mL DiI-labeled PFH@CL/Fe_3O_4 NPs. The connection between both groups was directly observed by confocal laser scanning microscopy (CLSM, Nikon A1, Japan). To quantitatively detect the connection rate of PFH@CL/Fe_3O_4 NPs and *B. bifidum*, the samples were divided into targeted group, non-targeted group, and *B. bifidum* control group, and the connection rate was detected by flow cytometry (FCM, BD FACSVantage SE, USA).

Cell Culture

The 4T1 breast cancer cells and vascular smooth muscle cells (VMSCs) were provided by the Institution of Ultrasound Imaging of Chongqing Medical University (The use of the cell lines was approved by the ethics committee of Chongqing Medical University). The cells were cultured in Roswell Park Memorial Institute-1640 (RPMI-1640) medium with 10% fetal bovine serum and 1% penicillin/streptomycin at 37°C and 5% CO_2.

Animal Model

Female BALB/c mice (4–6 weeks old, weight of 18–20 g) were provided by the Experimental Animal Center of Chongqing Medical University. All the experimental procedures were approved by the animal ethics committee of Chongqing Medical University. All procedures involving animals were conducted, following the guidelines of the Institutional Animal Care and Use Committee of Chongqing Medical University. To establish the tumor model, 1×10^6

4T1 cells suspended in 100 μL PBS was injected intravenously into the right thigh muscle of BALB/c mice. When the tumor volume reached 200 mm^3, the tumor-bearing mice were used.

In vivo Tumor Targeting Detection

Three tumor-bearing mice were randomly selected and injected intravenously with 200 μL *B. bifidum* (1×10^6 CFU/mL). All mice were sacrificed on day 7 after injection, and their heart, liver, spleen, lung, kidney, and tumor tissues were collected, homogenized, and smeared on BL Agar plates for anaerobic culture at 37°C. The biological distribution of *B. bifidum* in major organs and tumors was observed.

To further explore the tumor targeting ability of biological target NPs, tumor-bearing mice were randomly divided into targeted group and non-targeted group (three mice per group). In the targeted group, the mice were pre-injected intravenously with 200 μL *B. bifidum* (1×10^6 CFU/mL), and 200 μL of DiR-labeled PFH@CL/Fe_3O_4 NPs (1 mg/mL) was injected intravenously after 7 days. In the non-targeted group, 200 μL of PBS was injected in advance, and 200 μL of PFH@CL/Fe_3O_4 NPs (1 mg/mL) was injected after 7 days. The fluorescence signals of NPs in vivo were recorded at pre-injection, 6 h, 24 h, 30 h, and 48 h post-injection using LB983 NC320 in vivo imaging (Berthold Technologies GmbH & Co. KG, Germany). The tumors and major organs were collected, and in vitro fluorescence signal intensity was measured.

In vitro and in vivo Ultrasound Imaging

The liquid–gas phase transition of PFH in the NPs was observed under the optical microscope. A drop of PFH@CL/Fe_3O_4 NPs (1 mg/mL) was added to 10 mL Eppendorf tube and irradiated by HIFU exposure (Chongqing Haifu Medical Technology Co., Ltd., Chongqing, China). Vaporization of the NPs was observed before and after HIFU exposure.

For in vitro US imaging, four groups were divided as follows: PFH@CL/Fe_3O_4 NPs group, PFH/CL NPs group, Fe_3O_4/CL NPs group, and PBS group. The NPs of each group were transferred to 10-mL Eppendorf tubes and irradiated with HIFU (acoustic power 150 W, irradiation duration of 3 s). They were immediately transferred to 3% agarose gel (w/v) phantom. The US images under B mode and contrast-enhanced ultrasonography (CEUS) mode were acquired before and after HIFU irradiation using My LabCalssC advanced (Esaote, Italy). The gray value was measured using the DFY software (Institution of Ultrasound Imaging of Chongqing Medical University, China).

For in vivo US imaging, the 4T1 tumor-bearing mice were randomly divided into four groups (three mice per group): PBS, *B. bifidum*, PFH@CL/Fe_3O_4 NP, and *B. bifidum* + PFH@CL/Fe_3O_4 NP groups. The *B. bifidum* group and *B. bifidum* + PFH@CL/Fe_3O_4 NPs group were intravenously injected with 200 μL *B. bifidum* (1×10^6 CFU/mL), whereas the PBS group and PFH@CL/Fe_3O_4 NPs group were intravenously injected with 200 μL PBS. After 7 days, the mice in the PFH@CL/Fe_3O_4 NPs group and *B. bifidum* + PFH@CL/Fe_3O_4 NPs group were intravenously injected with 200 μL PFH@CL/Fe_3O_4 NPs (1 mg/mL). The PBS group and *B. bifidum* group were intravenously injected with 200 μL PBS. At 30 h post-injection (according to the in vivo fluorescence results), US images of tumor region of interest (ROI) were obtained before and after HIFU irradiation, and average gray of each tumor was quantitatively measured using the DFY software.

In vitro and in vivo Magnetic Resonance Imaging

For in vitro MRI performance, the PFH@CL/Fe_3O_4 NPs at various concentrations of Fe_3O_4 (20, 40, 100, 250, and 500 μg/mL) were resuspended in 3% agarose gel and placed in 2 mL Eppendorf tubes for T_2-weighted MRI (Bruker 7.0 T MRI scanner, Germany). T_2-weighted imaging parameters were set as: TE = 27 ms, TR = 2500 ms, slice thickness = 2.0 mm, FOV = 40 mm × 40 mm, and flip = 180°. The T_2 signal intensity (SI) of ROI in each group was measured.

For in vivo MRI, 4T1 tumor-bearing mice were randomly divided into targeted group (*B. bifidum*+ PFH@CL/Fe_3O_4 NPs (1 mg/mL)) and non-targeted group (PFH@CL/Fe_3O_4 NPs (1 mg/mL)), three mice per group. The T_2-weighted images were acquired at pre-injection, 6 h, 24 h, 30 h, and 48 h post-injection. The T_2-weighted imaging parameters were set as follows: TE = 45 ms, TR = 2500 ms, slice thickness = 1.0 mm, FOV = 35 mm × 25 mm, and flip = 180°. The T_2 SI in the tumor region (SI_{tumor}) was measured. The percentage of signal intensity decrease (PSID) was used to assess MRI effectiveness, $PSID = (SI_{pre} - SI_{post})/SI_{pre} \times 100\%$.

Synergistic Effect for HIFU Ablation

The experimental details of the synergistic effect of HIFU therapy in vitro can be found in Supporting Information 1.2.

For the evaluation of HIFU synergistic therapy in vivo, 4T1 tumor-bearing mice were randomly divided into four groups (three mice per group): PBS+HIFU, *B. bifidum* + HIFU, PFH@CL/Fe_3O_4 NPs + HIFU, *B. bifidum* + PFH@CL/Fe_3O_4 NPs + HIFU (Refer to the grouping method of in Vivo US Imaging). Thirty hours after injection, the tumor site was ablated with HIFU irradiation (150 W, 3 s). Twenty-four hours after HIFU ablation, tumor tissues were stained with 2% 2.3, 5-triphenyltriazolium chloride (TTC) solution. The Gray Val 1.0 software of the HIFU device was used to record the Gray level changes in the ablation area of patients in the four groups before and after HIFU irradiation, and the ablation area V was calculated as follows: $V(mm^3) = (\pi/6) \times \text{length} \times \text{width} \times \text{depth}$. Furthermore, energy efficiency factor (EEF) was measured according to the equation: $EEF\ (J/mm^3) = \eta Pt/V$, where η (set to 0.7 in the instrument) represents the focusing coefficient of HIFU transducer, P (W) represents the total power of HIFU, and t (s) represents total ablation time.

Hematoxylin-eosin (H&E) staining and terminal deoxynucleotide transferase-mediated notched-end labeling (TUNEL) were used to observe antitumor effects. A day after HIFU treatment, 4T1 tumor-bearing mice were euthanized, and tumor tissues were placed in 4% paraformaldehyde for H&E staining to observe the degree of tumor necrosis. Apoptosis was observed by TUNEL assay.

Biocompatibility Evaluation of PFH@CL/Fe_3O_4 NPs

The cytotoxicity of PFH@CL/Fe_3O_4 NPs in vitro was detected by the traditional MTT method. VMSC cells and 4T1 cells were cultured in 96-well plates (1×10^4 cells per well) for 24 h, and different concentrations of NPs (0.1, 0.5, 1, 2.5, and 5 mg/mL) were added to each well plate for 24 h. Thereafter, 20 μL of MTT solution (5 mg/mL) was added and incubated for 4 h. Finally, dimethyl sulfoxide (DMSO) was added to the solution and mixed. Additionally, the absorbance of each well was measured using a microplate reader (BIO-TEKEL × 800, USA) at 490 nm. Cell viability (%) was calculated using the following equation:

$$\text{Cell viability} = (OD_{\text{Cells+ NPs}} - OD_{\text{blank}})/(OD_{\text{Cells}} - OD_{\text{blank}}) \times 100\%$$

The experimental details of the Hemolysis test can be found in Supporting Information 1.3.

For evaluating in vivo toxicity, female BALB/c mice (18–20 g) were randomly divided into the biological target NP group and control group (three mice per group). Blood samples were collected 3, 7, and 14 days after injection of biological target NPs for biochemical examinations, including complete blood count of white blood cells (WBC), hemoglobin (HGB), red blood cells (RBC), and platelets (PLT); liver function markers, including alanine aminotransferase (ALT) and aspartate transaminase (AST); kidney function markers, such as creatinine (CREA), blood urea nitrogen (BUN), myocardial enzyme-spectrum lactate dehydrogenase (LDH), and creatine kinase (CK). After 14 days, the major organs (heart, liver, spleen, lung, and kidney) were stained with H&E for histological analysis and observed under an optical microscope.

Statistical Analysis

All data were analyzed using the IBM SPSS 25.0 software. Statistical data are presented as mean ± standard deviation (SD). Multi-group comparisons were analyzed using one-way ANOVA analysis, and differences between individual groups were determined using the LSD test (NS, no significance, *$p < 0.05$, **$p < 0.01$, ***$p < 0.001$).

Results and Discussion

PFH@CL/Fe_3O_4 NPs for *B. bifidum*-Mediated HIFU Ablation

Herein, as shown in Scheme 1, the *B. bifidum*-mediated strategy was designed to deliver PFH@CL-Fe_3O_4 NPs by electrostatic adsorption to solid tumors, resulting in enhanced efficiency of HIFU treatment due to the tumor-targeting ability of *B. bifidum*. The pre-targeting technique was used to verify the tumor-targeting ability of *B. bifidum* and stimulate the proliferation of *B. bifidum* in tumors to become targets of nanoparticles. Specifically, in the first step, *B. bifidum* was injected into mice bearing 4T1 xenografts with intravenous injection once every 24 h, three times in total.

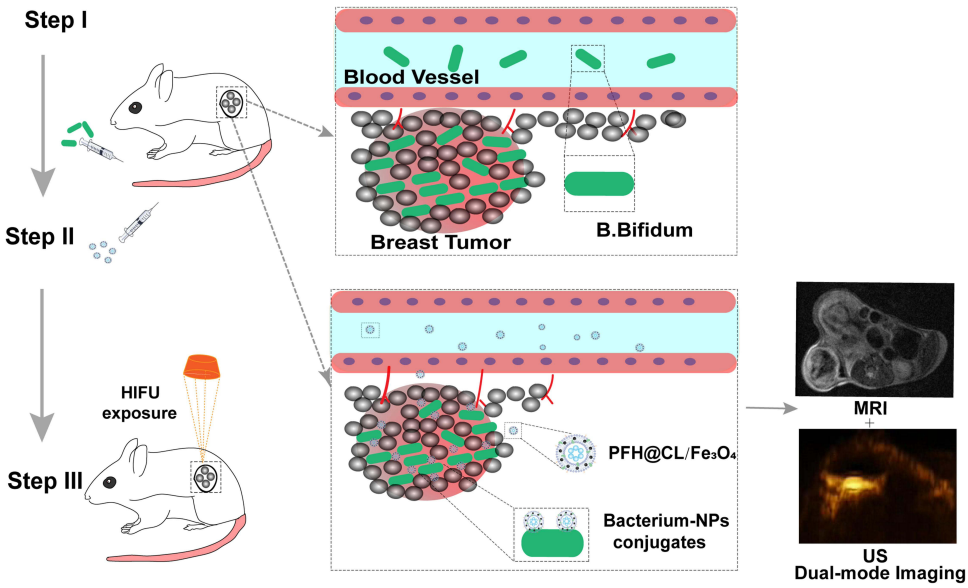

Scheme 1 Schematic illustration of *B.bifidum*-mediated PFH@CL-Fe_3O_4 targeted NPs for HIFU ablation and US/MR imaging.
Abbreviations: PFH, perfluorocarbon; Fe_3O_4, superparamagnetic iron oxide; PFH@CL-Fe_3O_4 NPs, PFH and Fe_3O_4 coloaded cationic lipid nanoparticles; *B.Bifidum, Bifidobacterium bifidum* strain ATCC29521; HIFU, High intensity focused ultrasound.

In the second step, after 7 days, PFH@CL-Fe_3O_4 NPs were injected again. Due to the negative potential of the surface of *B. bifidum*, cationic lipid NPs were aggregated into the tumor target area by electrostatic adsorption. This enabled targeted multimodal imaging in conjunction with HIFU therapy of tumors. Compared with the traditional HIFU synergistic agents, the novel bio-targeted nanoplatform had the advantages of good tumor targeting, temperature-sensitive phase transition, and HIFU ablation guided by ultrasound and MR, which is expected to become a new candidate method for HIFU ablation.

Synthesis and Characterization of PFH@CL/Fe_3O_4 NPs and *B. bifidum*

The PFH@CL/Fe_3O_4 NPs were synthesized through the thin film hydration method to concurrently encapsulate Fe_3O_4 and inert PFH as the core of the NPs (Figure 1A). The uniform lipid membranes included DPPC, DSPE-PEG (2000), DC-CHOL, and Fe_3O_4. The inner PFH was stably encapsulated in the membranes by the emulsification approach, forming PFH@CL/Fe_3O_4 NPs of PFH and Fe_3O_4. The resultant PFH@CL/Fe_3O_4 NPs had a regular spherical morphology and good dispersity in optical microscopy and TEM images, and Fe_3O_4 NPs were efficiently embedded in the spherical shell (Figure 1B and C). The Gram stain films of *B. bifidum* were observed under an optical microscope (Figure 1D). The average zeta potentials of PFH@CL/Fe_3O_4 NPs and *B. bifidum* were +23.2 ± 7.0 mV and −19.8 ± 5.3 mV, respectively (Figure 1E and F). The results indicated that they could be connected by electrostatic adsorption.

The PFH@CL/Fe_3O_4 NPs were relatively uniform nanospheres with a diameter of 267.4 ± 65.2 nm (PDI = 0.015) (Figure 1G). NPs can invade the vascular endothelial space to reach the core of tumor tissues. The PEGylation of lipid NPs prevent clearance by the mononuclear phagocytic system of the liver and spleen, which increases the circulation time of NPs.[32] Furthermore, the long-term stability of PFH@CL/Fe_3O_4 NPs was evaluated. The diameter and zeta potential of NPs remained stable within 9 days (Figure 1H and I), indicating the desirable long-term stability of the prepared nanocomposites. Liposomes have a good hydrophobicity and bilayer structure of phospholipid molecules; therefore, they are considered as ideal drug delivery vectors.[33,34] The Fe_3O_4 NPs content in the PFH@CL/Fe_3O_4 NP package was 221.0±12.8 μg/mL, and the loading efficiency was 88.4% wt% by atomic absorption spectrometry, which provided a possible use of nanoparticles in MRI.[35,36]

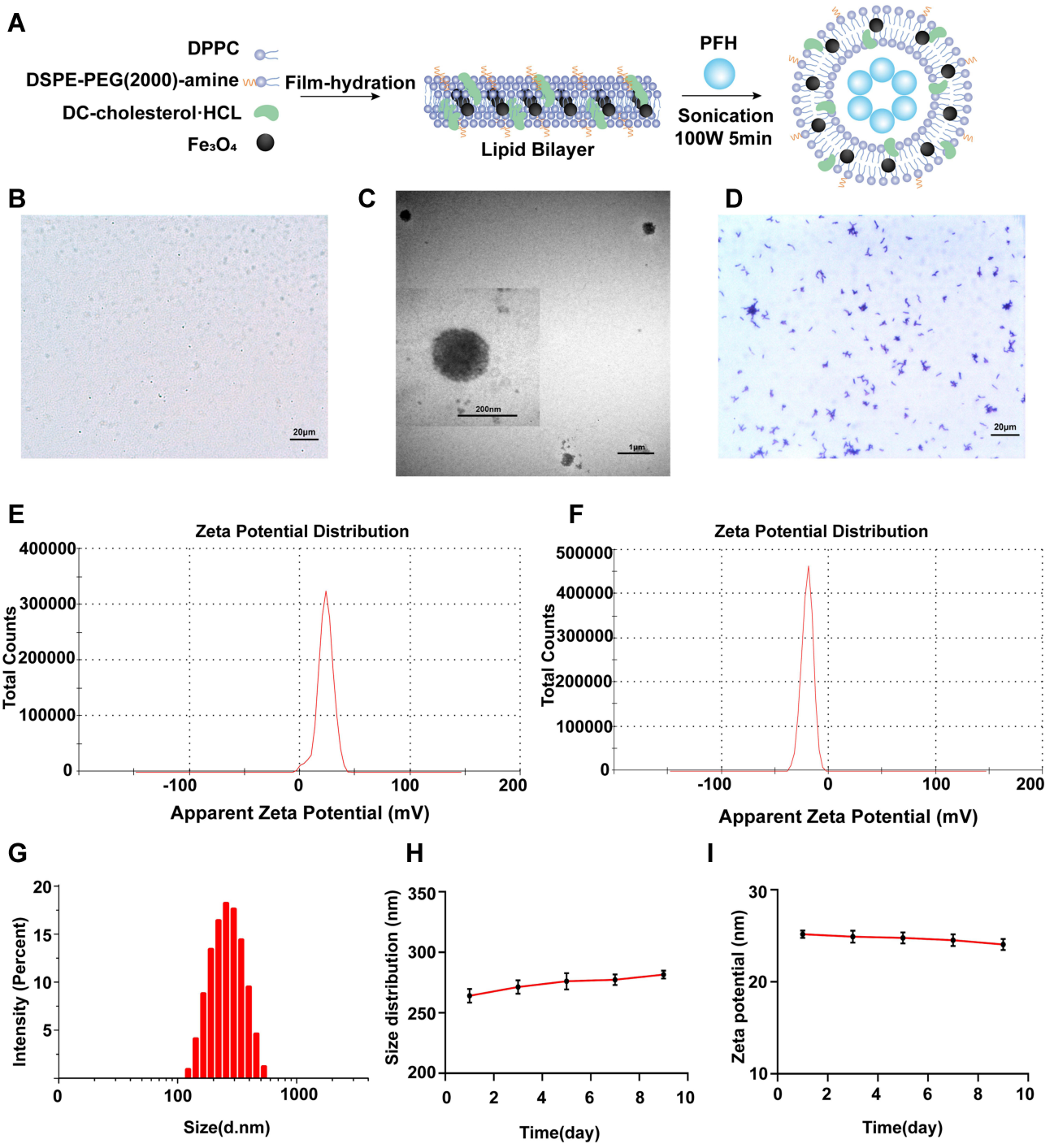

Figure 1 Synthesis and characterization of PFH@CL/Fe_3O_4 NPs and *B.Bifidum*. (**A**) Synthetic procedures for PFH@CL/Fe_3O_4 NPs via thin film hydration method. (**B**) Optical microscope image of PFH@CL/Fe_3O_4 NPs (400 × magnification), the scale bar is 20 μm. (**C**) TEM images of PFH@CL/Fe_3O_4 NPs. (**D**) Optical microscope image of Gram stain of *B.Bifidum* (400 × magnification), the scale bar is 20 μm. (**E**) Surface zeta potential of PFH@CL/Fe_3O_4 NPs. (**F**) Surface zeta potential of *B.Bifidum*. (**G**) Particle size distribution of PFH@CL/Fe_3O_4 NPs. (**H**) The particle size PFH@CL/Fe_3O_4 NPs over a period of 9 days in deionized water. (**I**) The zeta potential of NPs over a period of 9 days in deionized water.

Abbreviations: Fe_3O_4, Superparamagnetic Iron Oxide; PFH, perfluorohexanes; CL, cationic liposome; NPs, nanoparticles; HIFU, high-intensity focused ultrasound; TEM, transmission electron microscopy.

In vitro Construction of Biological Target Magnetic NPs

Herein, *B. bifidum* had a negative charge on its surface, whereas the NPs had a positive charge. Therefore, *B. bifidum* can be connected to PFH@CL/Fe_3O_4 NPs by electrostatic adsorption. Unlike the smooth surface *B. bifidum* (Figure S1A), the

B. bifidum + PFH@CL/Fe_3O_4 NPs consisted of PFH@CL/Fe_3O_4 NPs adhering to the surface of *B. bifidum* (Figure S1B). The particle size of *B. bifidum* alone was 955.4±28.74 nm (PDI = 0.153) (Figure S2A), and the *B. bifidum* coupled PFH@CL/Fe_3O_4 NPs was 1258.39±37.8 nm (PDI = 0.191) (Figure S2B). Furthermore, the conjugation of *B. bifidum* and PFH@CL/Fe_3O_4 NPs was evaluated by the CLSM method. Compared with the non-targeted group, the targeted group had several DiI-labeled red fluorescence PFH@CL/Fe_3O_4 NPs attached to the FITC-labeled green fluorescence *B. bifidum*, showing an orange fluorescence signal (Figure 2A). The conjugation efficiency of PFH@CL/Fe_3O_4 NPs and *B. bifidum* was detected using FCM. The results indicated that the connection rate was 97.95% in the targeted group and 1.29% in the non-targeted group (Figure 2B). These results indicated that *B. bifidum* and PFH@CL/Fe_3O_4 NPs successfully synthesized biological target magnetic NPs, which confirmed that the *B. bifidum* binds to cationic liposome NPs through electrostatic adsorption.[26,27,37]

Targeting Ability of Biological Target Magnetic NPs

To elaborate the distribution of *B. bifidum* in vivo 7 days after intravenous injection, the mice were sacrificed, and major organs (heart, liver, spleen, lung, kidney, and tumor tissues) were homogenized. Bacteria were colonized in the tumor tissues. In contrast, the main normal organs were bacteria-free (Figure 3A). Our research group confirmed that *B. bifidum* can specifically target tumor tissues and reproduce in a hypoxic tumor microenvironment.[22] These results suggest that *B. bifidum* can actively target and colonize tumor tissues.[38] Anaerobic *B. bifidum* readily proliferates in the anaerobic zone of the tumor after intravenous injection, which may be due to selective colonization of anaerobic bacteria in the hypoxic, immunosuppressive, and unique tumor microenvironment.[39]

To further evaluate the tumor targeting accumulation and distribution of biological target magnetic NPs in vivo, the fluorescence distribution of DiR-labeled PFH@CL/Fe_3O_4 NPs in mice was detected 6 h after intravenous injection. Fluorescence intensity of the targeted group increased gradually with time and reached the maximum at 30 h post-injection. Importantly, with the extension of time to 48 h after injection, a strong fluorescence intensity signal could still be observed, indicating that DiR-labeled PFH@CL/Fe_3O_4 NPs of the targeted group could remain in the tumor site (Figure 3B). The fluorescence intensity of the targeted group was significantly higher than that of the non-targeted group (Figure 3C), demonstrating that *B. bifidum* effectively targets PFH@CL/Fe_3O_4 NPs and prolongs its tumor accumulation time. In addition, major organs and tumors were harvested at 48 h post-injection to further confirm the accumulation of PFH@CL/Fe_3O_4 NPs in tumor tissues. As shown in in vitro imaging (Figure 3D), the liver and spleen had strong fluorescence signals in both groups, which was attributed to uptake effects of the reticuloendothelial system.[40] The fluorescence intensity of the targeted group at the tumor resection site was significantly stronger than that of the non-targeted group (Figure 3E). These results suggest that *B. bifidum* cloned at the tumor site could effectively retain PFH@CL/Fe_3O_4 NPs. This phenomenon may be related to the following factors: the proliferation of the bifidobacterium in tumors can increase vascular permeability and retention by increasing nitric oxide levels. Therefore, PFH@CL/Fe_3O_4 NPs easily penetrate the vascular endothelium and enter tumor tissues.[41,42]

All of the above phenomena prove that the *B. bifidum* can target and reproduce in tumor anoxic areas to retain more PFH@CL/Fe_3O_4 NPs. Therefore, the increasing therapeutic agents can enhance targeted imaging effect.

In vitro and in vivo Ultrasound Imaging

First, the phase transition of HIFU-induced NPs was studied to evaluate the US imaging capability of PFH@CL/Fe_3O_4 NPs. The imaging ability of PFH@CL/Fe_3O_4 NPs before and after irradiation was observed under an optical microscope. After irradiation, NPs enlarged and fused into microbubbles (Figure 4A). The PFH contained in PFH@CL/Fe_3O_4 NPs were simulated and heated by HIFU irradiation, resulting in liquid-gas phase transition of NPs and formation of large microbubbles. Ultrasonic imaging B-mode and CEUS-mode were used to observe the ability of NPs to form microbubbles (Figure 4B). Before HIFU irradiation, no obvious echogenicity was present in the CEUS-mode. However, after HIFU irradiation, significant differences were present in the CEUS-mode of each group, which confirmed the formation of bubbles in the mixture. Notably, the gray value of CEUS in the PFH@CL/Fe_3O_4 NP group was significantly higher than that in the PFH/CL, Fe_3O_4/CL and PBS groups (***$p < 0.001$) (Figure 4C), suggesting that combination of Fe_3O_4 NPs and PFH could accelerate the formation of bubbles.[43] Thereafter, US images of tumors were obtained to detect

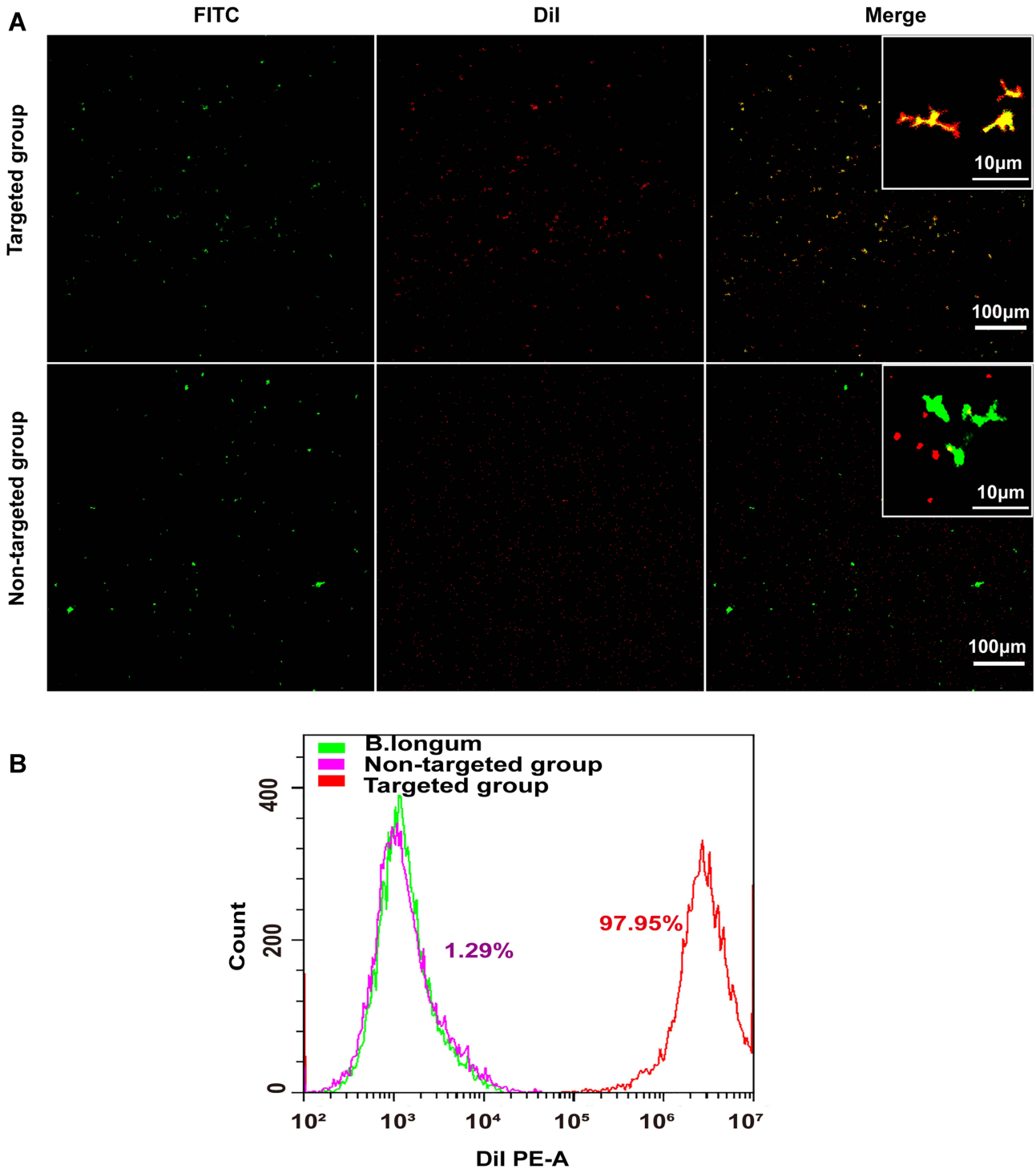

Figure 2 In vitro construction of the biological targeting magnetic NPs. (**A**) CLSM images of DiI-labeled cationic and non-cationic NPs (red) and FITC-labeled *B.Bifidum* (green). Compared with the non-targeted group, there was a significantly stronger red fluorescent signal on the surface of *B.Bifidum* in the targeted group, the scale bar is 100 μm. (**B**) FCM image of binding efficiencies of PFH@CL/Fe_3O_4 NPs and *B.Bifidum*.

Abbreviations: Fe_3O_4, Superparamagnetic Iron Oxide; PFH, perfluorohexanes; CL, cationic liposome; NPs, nanoparticles; *B.Bifidum, Bifidobacterium bifidum* strain ATCC 29521; FITC, fluorescein isothiocyanate; DiI, 1,1′-dioctadecyl-3,3,3′,3′-tetramethy lindocarbocyanine perchlorate; CLSM, confocal laser scanning microscope.

where PFH@CL/Fe_3O_4 NPs could be viewed by US imaging. In vivo ultrasound imaging of each group was observed before and after HIFU irradiation (Figure 4D). Before HIFU exposure, no significant difference in echo intensity of the CEUS-mode was present in each group. However, the echo intensity of the CEUS-mode in the *B. bifidum*+

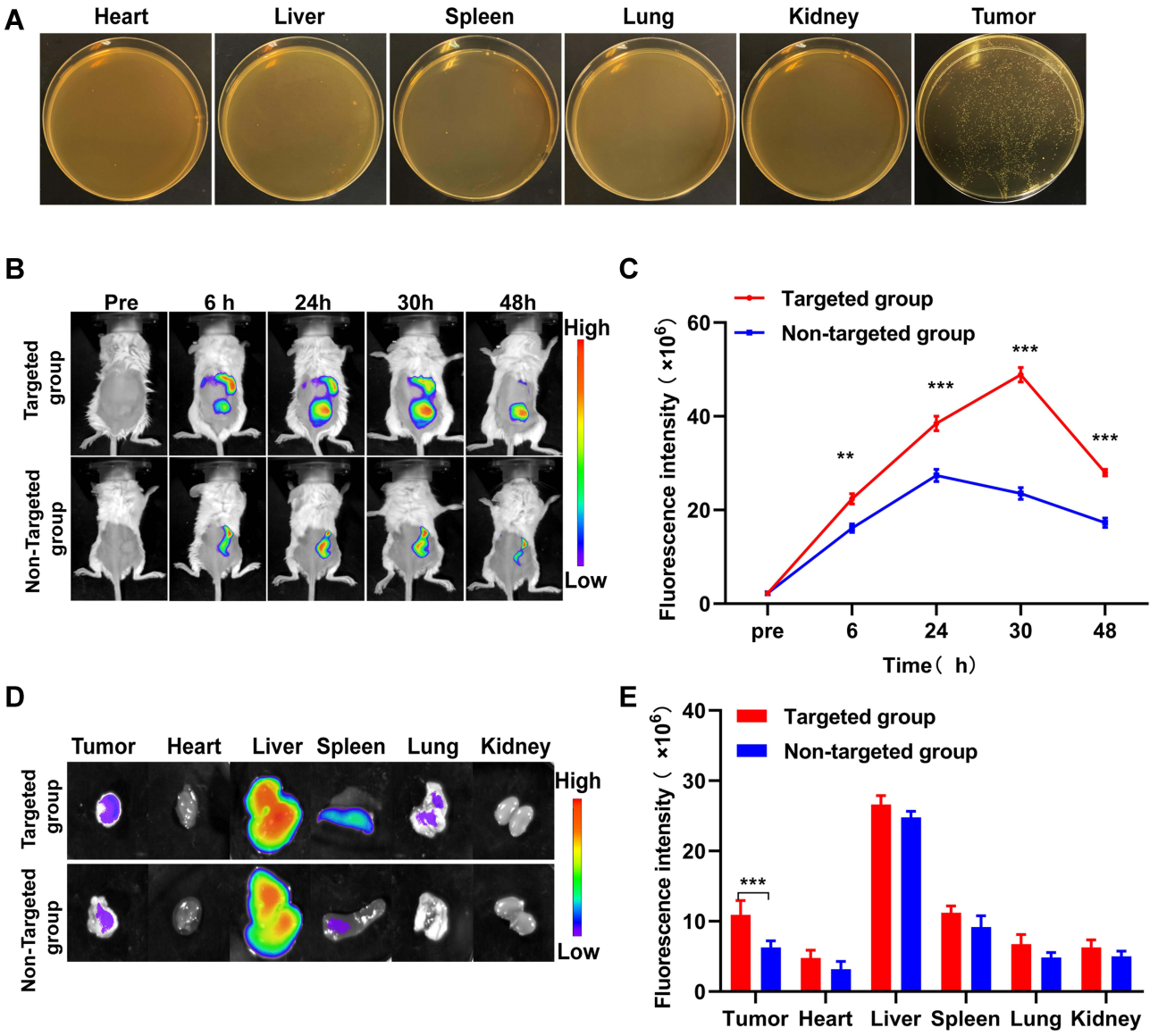

Figure 3 In vivo targeting behaviors of biological targeting magnetic NPs. (**A**) Homogenates of tumor tissues and normal organs were cultured on solid BL agar. (**B**) In vivo targeting efficiency before and after PFH@CL/Fe_3O_4 NPs with intravenous administration. Fluorescence intensity of tumor-bearing mice at pre-injection and 6h, 24h, 30h, 48h post-injection of targeted group and non-targeted group. (**C**) The corresponding in vivo quantitative fluorescence intensity of tumor. The fluorescence intensity in targeted group was slightly higher than that in non-targeted group 6h after injection of NPs (**p < 0.01). The fluorescence intensity in targeted group was significantly higher than that in non-targeted group 30h after injection of NPs (***p < 0.001). (**D**) In vitro fluorescence intensity of the major organs (heart, liver, spleen, lung and kidney) and tumors 48h after injection of targeted group and non-targeted group. (**E**) The corresponding in vitro quantitative fluorescence intensity of major organs and tumors. The fluorescence intensity of tumor in targeted group was significantly higher than that in non-targeted group (***p < 0.001).

Abbreviations: Fe_3O_4, Superparamagnetic Iron Oxide; PFH, perfluorohexanes; CL, cationic liposome; NPs, nanoparticles; *B.Bifidum, Bifidobacterium bifidum* strain ATCC 29521; FITC, fluorescein isothiocyanate.

PFH@CL/Fe_3O_4 NPs group after HIFU exposure was significantly higher than that before irradiation (***p < 0.001). In addition, the gray value of the CEUS-mode in the *B. bifidum* + PFH@CL/Fe_3O_4 NPs group was higher than that in the PFH@CL/Fe_3O_4 NP, *B. bifidum*, and PBS groups (***p < 0.001) (Figure 4E).

This phenomenon may be related to the following factors. First, PFH@CL/Fe_3O_4 NPs can strongly absorb ultrasonic energy and create heat under HIFU irradiation, leading to the liquid-gas phase transition of PFH to produce bubbles. Concurrently, the ultrasonic pressure wave generated by the thermal expansion of the tissues increases the acoustic signal.[44] Second, *B. bifidum* implanted in the tumor tissue enhances the deposition and retention of PFH@CL/Fe_3O_4 NPs, resulting in an increase in the echo intensity of the tumor target. As a result, the biological target magnetic NPs can provide more detailed information about tumors after intravenous injection and effectively guided tumor therapy.

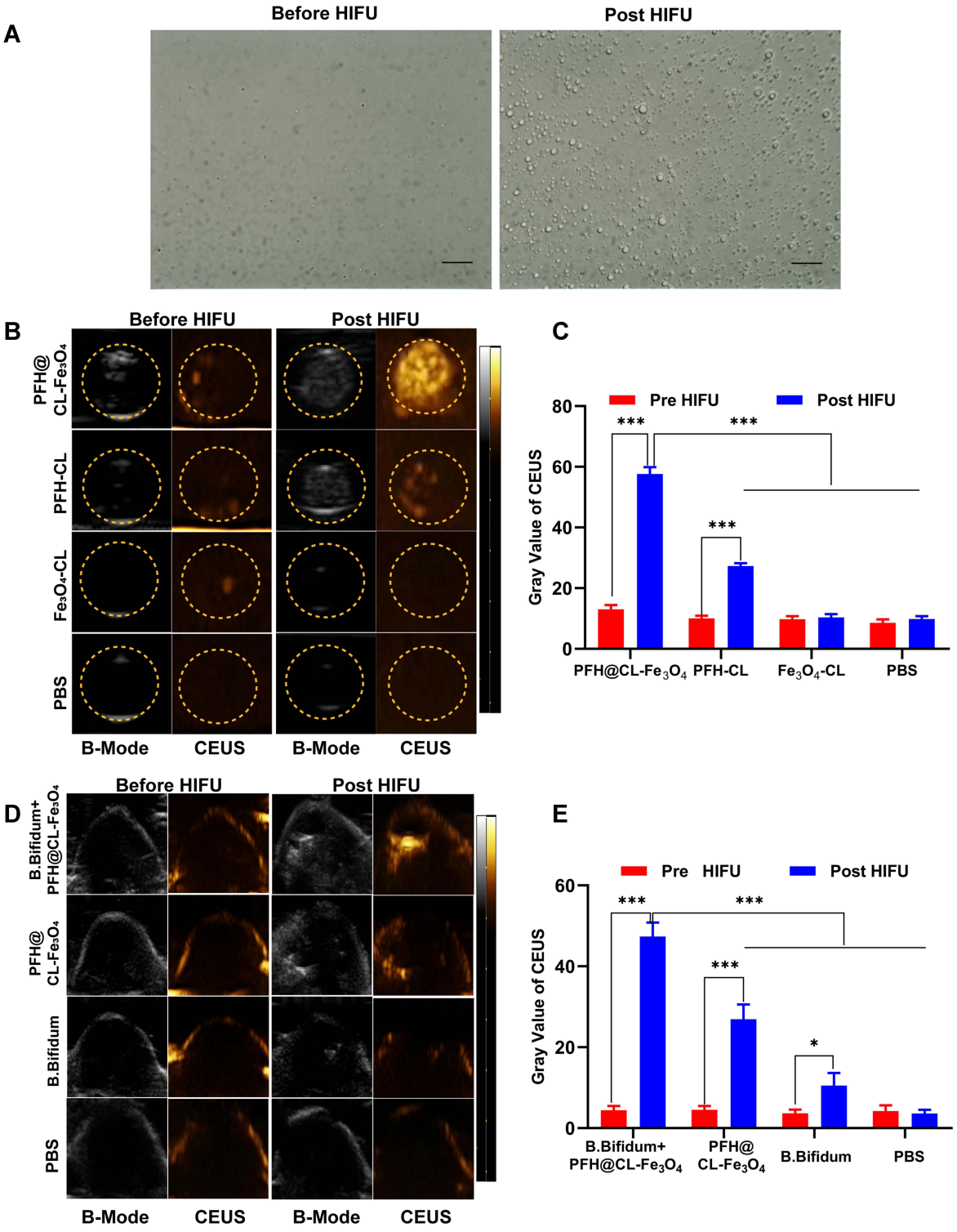

Figure 4 The phase transition of biological targeting NPs and contrast-enhanced ultrasound imaging both in vitro and in vivo. (**A**) Optical microscope image of PFH@CL/Fe_3O_4 NPs before and after HIFU irradiation (400 ×magnification). After irradiation, the NPs became larger and fused into microbubble, the scale bar is 20 μm. (**B**) In vitro ultrasound images of PFH@CL-Fe_3O_4, PFH-CL, Fe_3O_4-CL, PBS before and after HIFU irradiation. (**C**) The gray value of in vitro CEUS before and after HIFU irradiation (n = 3). The gray value of PFH@CL-Fe_3O_4 was significantly higher than those of other groups after HIFU irradiation (***p < 0.001). (**D**) In vivo B-mode and CEUS images of *B.Bifidum* + PFH@CL-Fe_3O_4, PFH@CL-Fe_3O_4, *B.Bifidum* and PBS before and after HIFU irradiation. (**E**) The gray value of in vivo CEUS before and after HIFU irradiation (n=3). The CEUS gray value of *B.Bifidum* group after HIFU ablation was slightly higher than that before HIFU ablation (*p < 0.05), and the CEUS gray value of *B. Bifidum* + PFH@CL-Fe_3O_4 group and PFH@CL-Fe_3O_4 group after HIFU ablation was significantly higher than that before ablation (***p < 0.001). After HIFU ablation, the CEUS gray value of *B.Bifidum* + PFH@CL-Fe_3O_4 group was significantly higher than that of the other three groups (***p < 0.001).

Abbreviations: Fe_3O_4, Superparamagnetic Iron Oxide; PFH, perfluorohexanes; CL, cationic liposome; NPs, nanoparticles; *B.Bifidum, Bifidobacterium bifidum* strain ATCC 29521; US, ultrasound; B-mode, brightness modulation; CEUS, contrast-enhanced ultrasound.

In vitro and in vivo Magnetic Resonance Imaging

Superparamagnetic Fe_3O_4 is an ideal contrast agent for T2-weighted MRI. The capability of PFH@CL/Fe_3O_4 NPs to entrap Fe_3O_4 NPs for MR imaging was verified in vitro. The different concentrations of PFH@CL/Fe_3O_4 NPs exhibited negative enhancement on T2-weighted MR images. In addition, MRI signal intensity decreased with the increase in Fe_3O_4 concentration (Figure 5A), confirming the ability of Fe_3O_4 in PFH@CL/Fe_3O_4 NPs to enhance MRI as a T2-weighted contrast agent. The r_2 values of PFH@CL/Fe_3O_4 NPs at different concentrations were quantitatively compared using the inverse relaxation time diagram ($1/T_2$). Furthermore, the in vivo MRI potential of PFH@CL/Fe_3O_4 NP, as a contrast agent, was evaluated. Negative dark effects were observed of tumor in the targeted group 6 h after intravenous injection (red circle callout) compared with the untargeted group (Figure 5B). The percentage of signal intensity reduction (SI dec) was used to quantitatively analyze the MRI signal intensity. The T2-weighted signal intensity of the targeted group decreased by 34% and reached its lowest value at 30 h post-injection. Decreased signaling persisted in the tumor up to 48 h after injection due to active targeted accumulation of PFH@CL/Fe_3O_4 NPs at the tumor site (Figure 5C). The superparamagnetic Fe_3O_4 encapsulated in liposome is an ideal contrast agent for T2-weighted MRI,

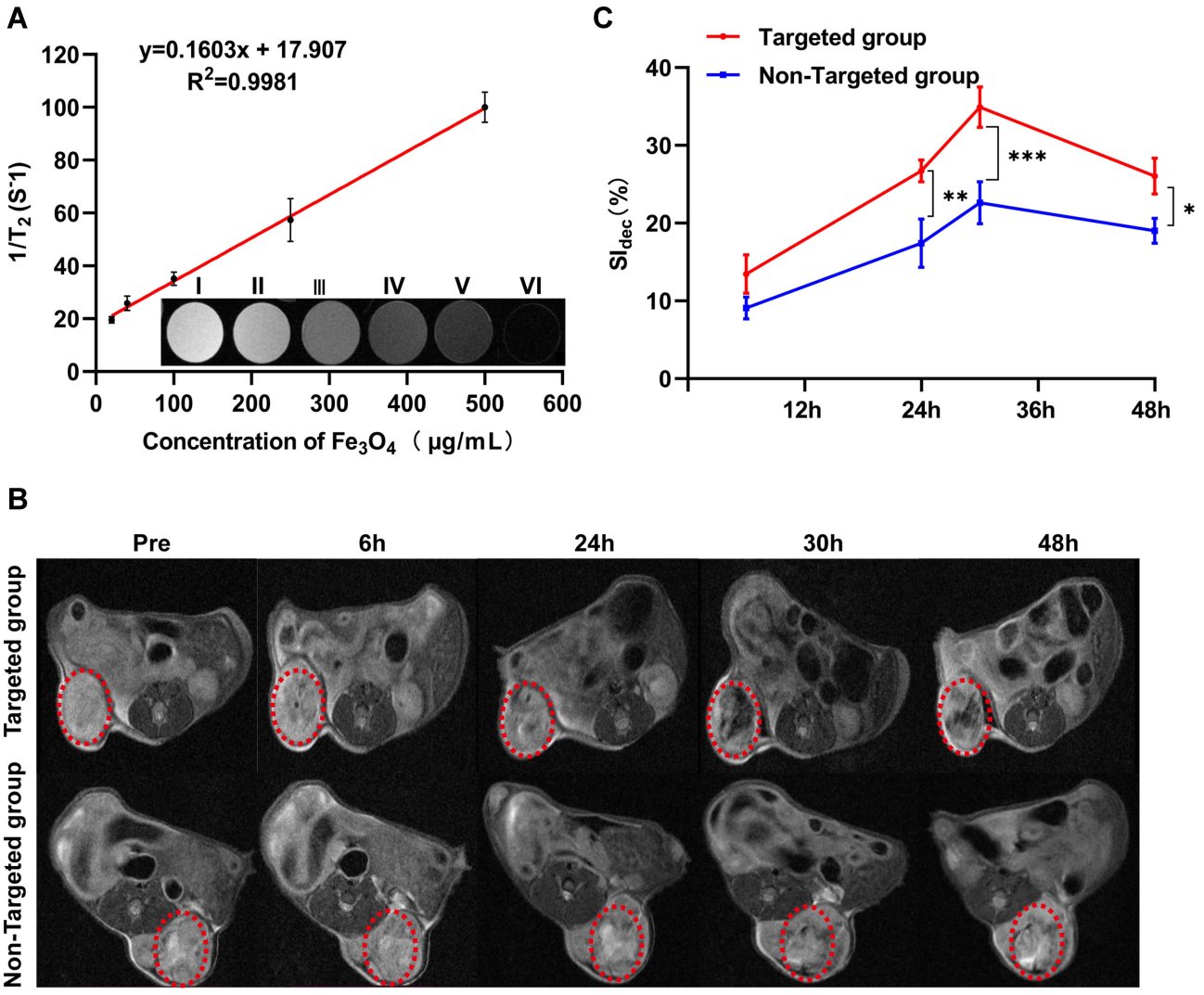

Figure 5 MRI assessment of PFH@CL/Fe_3O_4 NPs in vitro and in vivo. (**A**) The curve of $1/T_2$ versus PFH@CL/Fe_3O_4 NPs at elevated Fe_3O_4 concentration. Inset: T_2-weighted MR intensities of PFH@CL/Fe_3O_4 NPs at different Fe_3O_4 concentration (n = 3). (**B**) Image of 4T1 tumor-bearing mice (region enveloped by the red dotted line) at pre, 6h, 24h, 30h and 48h post-injection of targeted NPs and non-targeted NPs. (**C**) Quantitative analysis of SI_{dec} (n = 3), the difference was detected in the targeted group and non-targeted group (*p < 0.05, **p < 0.01, ***p < 0.001).

Abbreviations: Fe_3O_4, Superparamagnetic Iron Oxide; PFH, perfluorohexanes; CL, cationic liposome; NPs, nanoparticles; *B.Bifidum, Bifidobacterium bifidum* strain ATCC 29521; MRI, magnetic resonance imaging; SI, signal intensity.

which is conducive to accurate tumor diagnosis and can guide the selection of time windows and real-time monitoring during cancer therapy.[45,46]

Therefore, MR imaging results were similar to fluorescence imaging results, both in vitro and in vivo, suggesting that *B. bifidum*-mediated PFH@CL/Fe_3O_4 NPs can be retained in tumors and be used as a contrast agent for T2-weighted MRI. Bio-targeted nanoplatforms combined with *B. bifidum* and PFH@CL/Fe_3O_4 NPs can provide guidance and monitoring during HIFU therapy.

Synergistic Effect of PFH@CL/Fe_3O_4 NPs and HIFU Therapy

Encouraged by the distinct bubble-generation capability of PFH@CL/Fe_3O_4 NPs, the in vitro synergistic HIFU-based tumor ablation was evaluated by using ex vivo bovine livers (Figure S3A). Among these groups, the prepared NPs could improve the coagulative volume of HIFU ablation for ex vivo bovine livers (Figure S3B). In vivo synergistic effect of PFH@CL/ Fe_3O_4 NPs and HIFU irradiation in combating breast cancer was systematically evaluated. The treatment was initiated 30 h post-injection with different NPs, and the maximum concentration of *B. bifidum* + PFH@CL/Fe_3O_4 NPs in the tumor was observed by fluorescence imaging. After HIFU irradiation, the gray value of the tumor target region in all groups had varying degrees of change (Figure 6A). In addition, the gray value in the *B. bifidum* + PFH@CL/Fe_3O_4 NPs + HIFU group (Figure 6B) was higher than that in the other groups (***$p < 0.001$).

TTC staining indicated that the coagulative necrosis region of the ablated region was grayish-white, whereas the non-ablated region was red (Figure 6C). A clear separation was observed between the ablated and non-ablated areas in the *B. bifidum* + PFH@CL/Fe_3O_4 NPs + HIFU group and PFH@CL/Fe_3O_4 NPs group. The results suggest that PFH@CL/Fe_3O_4 NPs could damage the target tissues without affecting the adjacent normal tissues. The quantitative analysis of coagulative necrosis volume (Figure 6D) exhibited that the volume of the *B. bifidum* + PFH@CL/Fe_3O_4 NPs + HIFU group was significantly larger than that of the other groups (***$p < 0.001$). Moreover, the EEF values (Figure 6E) of the *B. bifidum* + PFH@CL/Fe_3O_4 NPs + HIFU group was markedly lower than those of the other groups (***$p < 0.001$). The introduction of microparticles or nanoparticles could change the acoustic environment of tissues, thus enhancing the acoustic energy deposition to improve the therapeutic efficiency of HIFU.[47] This was also confirmed in our study. This result indicated that under the same HIFU irradiation conditions, bio-targeted NPs had a stronger synergistic effect than the other treatment options because *B. bifidum* in tumor target areas capture several PFH@CL/Fe_3O_4 NPs. In addition, multimodal imaging can select the optimal treatment time based on the distribution of nanoparticles in vivo to guide the efficient and effective treatment of tumors.

To further validate the degree of tumor necrosis after HIFU ablation, two approaches of pathological examinations were applied. The H&E staining of the tumor tissues in the *B. bifidum* + PFH@CL/Fe_3O_4 NPs + HIFU group had the largest region of coagulative necrosis, and the gap between the ablation target region and non-ablation target region was clearly obvious, indicating the excellent ability of the biological target NPs in ablating tumors. In contrast, tumor cells in nests exhibited good cellular morphology in the PBS group. Moreover, for evaluating the tumor-cell proliferation and apoptosis levels of tumors after HIFU ablation, immunohistochemical staining with the TUNEL assays was performed (Figure 6F). Apoptosis can be induced by heat, cold and ultraviolet stimulation, which is a normal physiological process to maintain tissue homeostasis. Studies have shown that heat stress enhanced by microbubbles may be associated with more apoptotic events during HIFU exposure.[48] The results indicated that positive staining (brown nuclei) cells represented apoptotic cells, and the tumor tissues in the *B. bifidum* + PFH@CL/Fe_3O_4 NPs + HIFU group had the least number of brown proliferative cells by the TUNEL assay.

The above results prove that PFH@CL/Fe_3O_4 NPs could serve as HIFU synergistic agents. Moreover, *B. bifidum*-mediated PFH@CL/Fe_3O_4 can be retained in tumor target regions for longer durations, further enhancing the HIFU ablation efficiency.

Biosafety Assay

To evaluate the cytotoxicity of PFH@CL/Fe_3O_4 NPs, cell cytotoxicity using the MTT assay and in vivo toxicity in healthy BALB/c mice were analyzed. Cell viability results of 4T1 cells and VMSCs cells showed no significant cytotoxicity, the concentration of PFH@CL/Fe_3O_4 NPs increased to as high as 5 mg/mL (Figure 7A). Then, we conducted the hemolysis test to

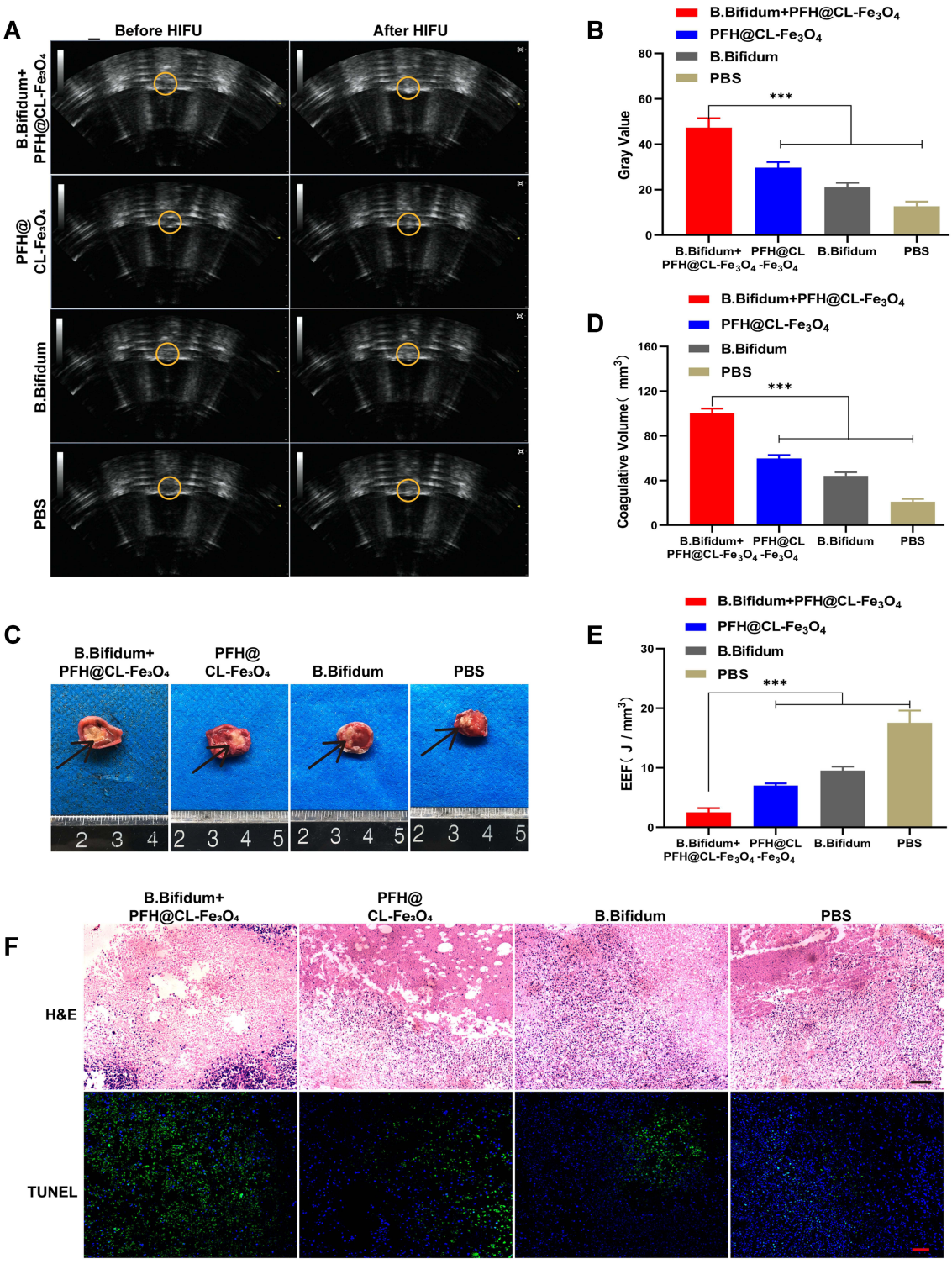

Figure 6 Synergistic HIFU treatment of PFH@CL/Fe_3O_4 NPs. (**A**) In vivo US imaging of tumor tissues (yellow circle) before and after HIFU irradiation in different group. The yellow dotted circle marks the tumor nodules. (**B**) The comparison of gray values of tumor tissues in each group after HIFU irradiation. The mean grayscale difference in the *B.Bifidum* + PFH@CL/Fe_3O_4 NPs group was significantly higher than the other groups (n = 3, *** p < 0.001). (**C**) Coagulative necrosis of tumors by TTC staining after HIFU therapy, the necrosis tissue appears grayish white (black arrow) and the normal tumor tissue is red. (**D**) The comparison of coagulative necrosis of tumor tissues in each group after HIFU irradiation. The coagulative necrosis volume of the *B.Bifidum* + PFH@CL/Fe_3O_4 NPs group was significantly bigger than any other groups (n = 3, ***p < 0.001). (**E**) The comparison of EEF of tumor tissues in each group after HIFU irradiation. The results showed that the *B.Bifidum* + PFH@CL/Fe_3O_4 NPs group was significantly lower than any other groups (n = 3, *** p < 0.001). (**F**) Optical microscope images of tumor sections from each group after HIFU ablation were stained for HE staining, TUNEL assay. There exists a significant boundary between the nonablated and ablated region in HE staining (200 × magnification), the scale bar is 20 μm. TUNEL positive cells are in brown and increased in the coagulation necrosis region (400 × magnification), the scale bar is 10μm.

Abbreviations: Fe_3O_4, Superparamagnetic Iron Oxide; PFH, perfluorohexanes; CL, cationic liposome; NPs, nanoparticles; *B.Bifidum, Bifidobacterium bifidum* strain ATCC 29521; HIFU, high-intensity focused ultrasound; TTC, 2, 3, 5-Triphenyte-trazoliumchloride; TUNEL, terminal-deoxynucleotidyl transferase-mediated nick end labeling.

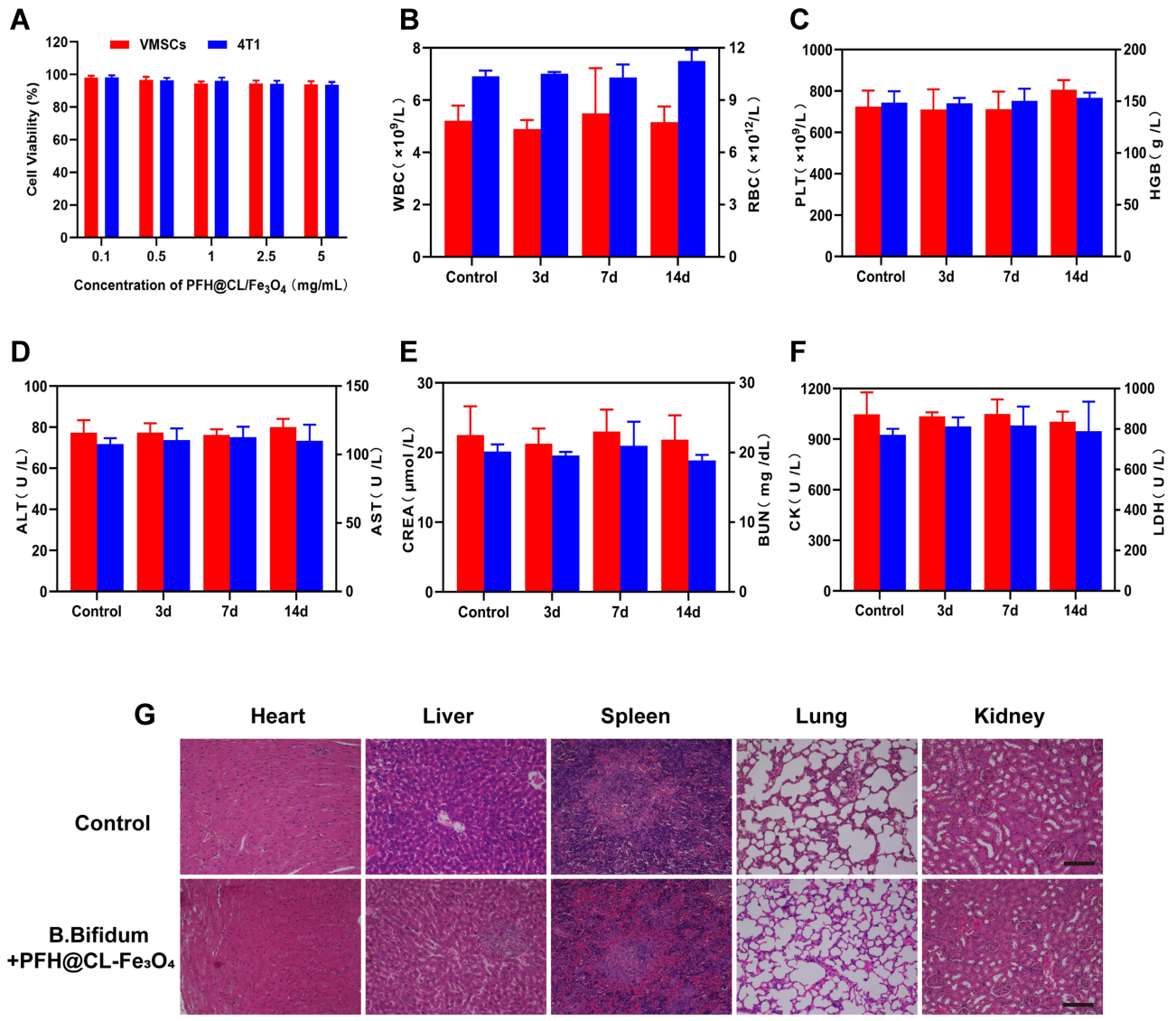

Figure 7 Biosafety assay. (**A**) Cell viability assay of different concentration PFH@CL/Fe_3O_4 NPs incubated with 4T1 breast tumor cells and VMSCs normal cells. (**B**–**F**) Hematological assay of BALB/c mice of control group and the experimental groups at the corresponding time point. (**G**) H&E staining in major organs (heart, liver, spleen, lung, and kidney) of control group and the experimental groups after HIFU ablation (H&E: ×200 magnification), the scale bar is 20 μm.
Abbreviations: HIFU, high-intensity focused ultrasound; H&E, hematoxylin and eosin staining.

evaluate the preliminary biocompatibility of PFH@CL/Fe_3O_4 NPs. Only a minor hemolysis rate (<5%) was observed when the PFH@CL/Fe_3O_4 NPs concentrates were as high as 5 mg/mL (Figure S4), indicating favorable biocompatibility of the nanocarriers for in vivo applications.

Furthermore, to evaluate the in vivo safety of biological target NPs, the blood biochemical indexes and H&E staining in mice were examined. The results of WBC, RBC, PLT, HGB (Figure 7B and C), ALT and AST (Figure 7D), BUN and CREA (Figure 7E), and CK and LDH (Figure 7F) indicated negligible differences among all groups at 3 days, 7 days, and 14 days post-injection, indicating that toxicity was undetectable in the mice during the tests. Additionally, the H&E staining analysis of the heart, liver, spleen, lung, and kidney revealed no noticeable damage with the use of biological target NPs (Figure 7G). These results reveal the high histocompatibility of biological target NPs.

Conclusion

This is the first study to report a *B. bifidum*-mediated strategy to deliver PFH@CL/Fe_3O_4 NPs by electrostatic adsorption approach into solid tumor under the dual-modal imaging (MR/US) guidance. These novel bio-targeting NPs were developed for synergistic HIFU therapy of tumors. Specifically, we successfully synthesized PFH@CL/Fe_3O_4 NPs using film hydration methods which can target *B.bifidum* colonized in tumor by electrostatic adsorption.[30,49,50] The elaborately designed bio-targeting NPs can achieve high tumor accumulation and significantly enhance HIFU therapeutic efficiency under the dual-modal imaging guidance. Compared with the typical cancer-treatment protocols, such as chemotherapy, *B. bifidum*-mediated strategy can significantly synergistic HIFU treatment for breast cancer. Futhermore, the US combined MR imaging performance is conducive to monitoring the reaction of tumor sites and guiding the selection of the HIFU irradiation time window during cancer therapy. Multimodal imaging integrates the advantages of individualized imaging modalities and provides more accurate biological information for the early diagnosis of tumors and monitoring of HIFU therapy.[51,52] However, the utility of this biologically targeted potentiator of HIFU for real-time monitoring and prognostic assessment through multimodal imaging should be further investigated in this study. In summary, this multimodal image-guided HIFU approach provides a promising strategy for the diagnosis and treatment of triple negative breast cancer and can be used as a safe clinical transformation method. In the future research, this bio-targeted approach could be used to guide US, MR and photoacoustic imaging multimodal nanomaterials and in combination with immunotherapy and chemotherapy for triple negative breast cancer.

Acknowledgments

Fujie Jiang and Lu Wang contributed equally to this work.

Disclosure

The authors report no conflicts of interest in this work.

References

1. Kennedy JE. High-intensity focused ultrasound in the treatment of solid tumours. *Nat Rev Cancer*. 2005;5(4):321–327. doi:10.1038/nrc1591
2. Diana M, Schiraldi L, Liu YY, et al. High intensity focused ultrasound (HIFU) applied to hepato-bilio-pancreatic and the digestive system-current state of the art and future perspectives. *Hepatobiliary Surg Nutr*. 2016;5(4):329–344. doi:10.21037/hbsn.2015.11.03
3. Duc NM, Keserci B. Emerging clinical applications of high-intensity focused ultrasound. *Diagn Interv Radiol*. 2019;25(5):398–409. doi:10.5152/dir.2019.18556
4. Elhelf IAS, Albahar H, Shah U, et al. High intensity focused ultrasound: the fundamentals, clinical applications and research trends. *Diagn Interv Imaging*. 2018;99(6):349–359. doi:10.1016/j.diii.2018.03.001
5. Cheung TT, Ma KW, She WH. A review on radiofrequency, microwave and high-intensity focused ultrasound ablations for hepatocellular carcinoma with cirrhosis. *Hepatobiliary Surg Nutr*. 2021;10(2):193–209. doi:10.21037/hbsn.2020.03.11
6. Al-Bataineh O, Jenne J, Huber P. Clinical and future applications of high intensity focused ultrasound in cancer. *Cancer Treat Rev*. 2012;38(5):346–353. doi:10.1016/j.ctrv.2011.08.004
7. Tang H, Guo Y, Peng L, et al. In vivo targeted, responsive, and synergistic cancer nanotheranostics by magnetic resonance imaging-guided synergistic high-intensity focused ultrasound ablation and chemotherapy. *ACS Appl Mater Interfaces*. 2018;10(18):15428–15441. doi:10.1021/acsami.8b01967
8. Zhang Y, Yong L, Luo Y, et al. Enhancement of HIFU ablation by sonosensitizer-loading liquid fluorocarbon nanoparticles with pre-targeting in a mouse model. *Sci Rep*. 2019;9(1):6982. doi:10.1038/s41598-019-43416-y
9. Chen Y, Chen H, Sun Y, et al. Multifunctional mesoporous composite nanocapsules for highly efficient MRI-guided high-intensity focused ultrasound cancer surgery. *Angewandte Chemie*. 2011;50(52):12505–12509.
10. Wang X, Chen H, Chen Y, et al. Perfluorohexane-encapsulated mesoporous silica nanocapsules as enhancement agents for highly efficient high intensity focused ultrasound (HIFU). *Adv Mater*. 2012;24(6):785–791. doi:10.1002/adma.201104033
11. Sabuncu S, Yildirim A. Gas-stabilizing nanoparticles for ultrasound imaging and therapy of cancer. *Nano Convergence*. 2021;8(1):39. doi:10.1186/s40580-021-00287-2
12. Yildirim A, Chattaraj R, Blum NT, et al. Stable encapsulation of air in mesoporous silica nanoparticles: fluorocarbon-free nanoscale ultrasound contrast agents. *Adv Healthcare Mater*. 2016;5(11):1290–1298. doi:10.1002/adhm.201600030
13. Ma M, Xu H, Chen H, et al. A drug-perfluorocarbon nanoemulsion with an ultrathin silica coating for the synergistic effect of chemotherapy and ablation by high-intensity focused ultrasound. *Adv Mater*. 2014;26(43):7378–7385. doi:10.1002/adma.201402969
14. Zhou Y, Wang Z, Chen Y, et al. Microbubbles from gas-generating perfluorohexane nanoemulsions for targeted temperature-sensitive ultrasonography and synergistic HIFU ablation of tumors. *Adv Mater*. 2013;25(30):4123–4130. doi:10.1002/adma.201301655
15. Sharma N, Singhal M, Kumari RM, et al. Diosgenin loaded polymeric nanoparticles with potential anticancer efficacy. *Biomolecules*. 2020;10(12):1679. doi:10.3390/biom10121679
16. Kumari M, Sharma N, Manchanda R, et al. PGMD/curcumin nanoparticles for the treatment of breast cancer. *Sci Rep*. 2021;11(1):3824. doi:10.1038/s41598-021-81701-x

17. Prasad KS, Pillai RR, Shivamallu C, et al. Tumoricidal potential of novel Amino-1,10-phenanthroline derived imine ligands: chemical preparation, structure, and biological investigations. *Molecules*. 2020;25(12):2865. doi:10.3390/molecules25122865
18. Sharma N, Kumari RM, Gupta N, et al. Poly-(Lactic-co-Glycolic) acid nanoparticles for synergistic delivery of epirubicin and paclitaxel to human lung cancer cells. *Molecules*. 2020;25(18):4243. doi:10.3390/molecules25184243
19. Lee SH, Cho SY, Yoon Y, et al. Bifidobacterium bifidum strains synergize with immune checkpoint inhibitors to reduce tumour burden in mice. *Nature Microbiol*. 2021;6(3):277–288. doi:10.1038/s41564-020-00831-6
20. Tang Y, Chen C, Jiang B, et al. Bifidobacterium bifidum-mediated specific delivery of nanoparticles for tumor therapy. *Int J Nanomedicine*. 2021;16:4643–4659. doi:10.2147/IJN.S315650
21. Liang K, Liu Q, Li P, et al. Genetically engineered Salmonella Typhimurium: recent advances in cancer therapy. *Cancer Lett*. 2019;448:168–181. doi:10.1016/j.canlet.2019.01.037
22. Wei B, Pan J, Yuan R, et al. Polarization of tumor-associated macrophages by nanoparticle-loaded escherichia coli combined with immunogenic cell death for cancer immunotherapy. *Nano Lett*. 2021;21(10):4231–4240. doi:10.1021/acs.nanolett.1c00209
23. Yang H, Jiang F, Ji X, et al. Genetically engineered bacterial protein nanoparticles for targeted cancer therapy. *Int J Nanomedicine*. 2021;16:105–117. doi:10.2147/IJN.S292432
24. Yazawa K, Fujimori M, Amano J, et al. Bifidobacterium longum as a delivery system for cancer gene therapy: selective localization and growth in hypoxic tumors. *Cancer Gene Ther*. 2000;7(2):269–274. doi:10.1038/sj.cgt.7700122
25. Taniguchi S, Fujimori M, Sasaki T, et al. Targeting solid tumors with non-pathogenic obligate anaerobic bacteria. *Cancer Sci*. 2010;101(9):1925–1932. doi:10.1111/j.1349-7006.2010.01628.x
26. Gao X, Zou W, Jiang B, et al. Experimental study of retention on the combination of bifidobacterium with High-Intensity Focused Ultrasound (HIFU) synergistic substance in tumor tissues. *Sci Rep*. 2019;9(1):6423. doi:10.1038/s41598-019-42832-4
27. Wang Y, Chen C, Luo Y, et al. Experimental study of tumor therapy mediated by multimodal imaging based on a biological targeting synergistic agent. *Int J Nanomedicine*. 2020;15:1871–1888. doi:10.2147/IJN.S238398
28. Luo CH, Huang CT, Su CH, et al. Bacteria-mediated hypoxia-specific delivery of nanoparticles for tumors imaging and therapy. *Nano Lett*. 2016;16(6):3493–3499. doi:10.1021/acs.nanolett.6b00262
29. Lee SY, Jeon SI, Jung S, et al. Targeted multimodal imaging modalities. *Adv Drug Deliv Rev*. 2014;76:60–78. doi:10.1016/j.addr.2014.07.009
30. Guo Y, Wang XY, Chen YL, et al. A light-controllable specific drug delivery nanoplatform for targeted bimodal imaging-guided photothermal/chemo synergistic cancer therapy. *Acta Biomater*. 2018;80:308–326. doi:10.1016/j.actbio.2018.09.024
31. Ye S, Liu Y, Lu Y, et al. Cyclic RGD functionalized liposomes targeted to activated platelets for thrombosis dual-mode magnetic resonance imaging. *J Mater Chem B*. 2020;8(3):447–453. doi:10.1039/C9TB01834D
32. Jin M, Jin G, Kang L, et al. Smart polymeric nanoparticles with pH-responsive and PEG-detachable properties for co-delivering paclitaxel and survivin siRNA to enhance antitumor outcomes. *Int J Nanomedicine*. 2018;13:2405–2426. doi:10.2147/IJN.S161426
33. Torchilin VP. Recent advances with liposomes as pharmaceutical carriers. *Nat Rev Drug Discov*. 2005;4(2):145–160. doi:10.1038/nrd1632
34. Lamichhane N, Udayakumar TS, D'Souza WD, et al. Liposomes: clinical applications and potential for image-guided drug delivery. *Molecules*. 2018;23(2):288. doi:10.3390/molecules23020288
35. Farzin A, Etesami SA, Quint J, et al. Magnetic nanoparticles in cancer therapy and diagnosis. *Adv Healthcare Mater*. 2020;9(9):e1901058. doi:10.1002/adhm.201901058
36. Jahangirian H, Kalantari K, Izadiyan Z, et al. A review of small molecules and drug delivery applications using gold and iron nanoparticles. *Int J Nanomedicine*. 2019;14:1633–1657. doi:10.2147/IJN.S184723
37. Xiao S, Shi H, Zhang Y, et al. Bacteria-driven hypoxia targeting delivery of chemotherapeutic drug proving outcome of breast cancer. *J Nanobiotechnology*. 2022;20(1):178. doi:10.1186/s12951-022-01373-1
38. Xu D, Zou W, Luo Y, et al. Feasibility between bifidobacteria targeting and changes in the acoustic environment of tumor tissue for synergistic HIFU. *Sci Rep*. 2020;10(1):7772. doi:10.1038/s41598-020-64661-6
39. Zhou H, He Z, Wang C, et al. Intravenous administration is an effective and safe route for cancer gene therapy using the bifidobacterium-mediated recombinant HSV-1 thymidine kinase and ganciclovir. *Int J Mol Sci*. 2016;17(6):891. doi:10.3390/ijms17060891
40. Fang J, Nakamura H, Maeda H. The EPR effect: unique features of tumor blood vessels for drug delivery, factors involved, and limitations and augmentation of the effect. *Adv Drug Deliv Rev*. 2011;63(3):136–151. doi:10.1016/j.addr.2010.04.009
41. Maeda H, Fang J, Inutsuka T, et al. Vascular permeability enhancement in solid tumor: various factors, mechanisms involved and its implications. *Int Immunopharmacol*. 2003;3(3):319–328. doi:10.1016/S1567-5769(02)00271-0
42. Chen C, Wang Y, Tang Y, et al. Bifidobacterium-mediated high-intensity focused ultrasound for solid tumor therapy: comparison of two nanoparticle delivery methods. *Int J Hyperthermia*. 2020;37(1):870–878. doi:10.1080/02656736.2020.1791365
43. Liu Y, Li J, Chen H, et al. Magnet-activatable nanoliposomes as intracellular bubble microreactors to enhance drug delivery efficacy and burst cancer cells. *Nanoscale*. 2019;11(40):18854–18865. doi:10.1039/C9NR07021D
44. Wang D, Jiang F, Wang L, et al. Polyethylenimine (PEI)-modified poly (lactic-co-glycolic) acid (PLGA) nanoparticles conjugated with tumor-homing bacteria facilitate high intensity focused ultrasound-mediated tumor ablation. *Biochem Biophys Res Commun*. 2021;571:104–109. doi:10.1016/j.bbrc.2021.07.061
45. Wang Y, Li X, Chen P, et al. Enzyme-instructed self-aggregation of Fe3O4 nanoparticles for enhanced MRI T2 imaging and photothermal therapy of tumors. *Nanoscale*. 2020;12(3):1886–1893. doi:10.1039/C9NR09235H
46. Liang X, Chen M, Bhattarai P, et al. Complementing cancer photodynamic therapy with ferroptosis through iron oxide loaded porphyrin-grafted lipid nanoparticles. *ACS Nano*. 2021;15(12):20164–20180. doi:10.1021/acsnano.1c08108
47. Chen Y, Chen H, Shi J. Nanobiotechnology promotes noninvasive high-intensity focused ultrasound cancer surgery. *Adv Healthc Mater*. 2015;4(1):158–165. doi:10.1002/adhm.201400127
48. Luo W, Zhou X, Zhang J, et al. Analysis of apoptosis and cell proliferation after high intensity-focused ultrasound ablation combined with microbubbles in rabbit livers. *Eur J Gastroenterol Hepatol*. 2007;19(11):158–165. doi:10.1097/MEG.0b013e3282cfb6f0
49. Li X, Fu GF, Fan YR, et al. Bifidobacterium adolescentis as a delivery system of endostatin for cancer gene therapy: selective inhibitor of angiogenesis and hypoxic tumor growth. *Cancer Gene Ther*. 2003;10(2):105–111. doi:10.1038/sj.cgt.7700530

50. Kimura NT, Taniguchi S, Aoki K, et al. Selective localization and growth of Bifidobacterium bifidum in mouse tumors following intravenous administration. *Cancer Res*. 1980;40(6):2061–2068.
51. Cai W, Chen X. Multimodality molecular imaging of tumor angiogenesis. *J nuclear med*. 2008;Suppl 49(Suppl 2):113s–128s. doi:10.2967/jnumed.107.045922
52. Kim J, Choi W, Park EY, et al. Real-time photoacoustic thermometry combined with clinical ultrasound imaging and high-intensity focused ultrasound. *IEEE Trans Biomed Eng*. 2019;66(12):3330–3338. doi:10.1109/TBME.2019.2904087